ChemComm

COMMUNICATION

View Article Online
View Journal | View Issue



Cite this: *Chem. Commun.*, 2020, **56**, 6344

Received 10th January 2020,
Accepted 20th April 2020

DOI: 10.1039/d0cc00233j

rsc.li/chemcomm



# An endoplasmic reticulum-targeting fluorescent probe for imaging •OH in living cells†

Yanyan Zhao,[ab] Hongyu Li,[a] Ziyin Chai,[a] Wen Shi,*[ab] Xiaohua Li[a] and Huimin Ma*[ab]

**The hydroxyl radical (•OH) in the endoplasmic reticulum has not been studied thoroughly due to the lack of proper methods. Here, an endoplasmic reticulum-targeting fluorescent probe for detecting •OH is reported. With this probe, the action of •OH in the endoplasmic reticulum has been imaged in living cells.**

Endoplasmic reticulum (ER), a membrane-like cellular organelle, forms an interconnected network of space in eukaryotes. It is primarily responsible for the translation, modification and delivery of protein, calcium homeostasis, and lipid metabolism.[1] ER is extremely sensitive to pathological insults such as inflammation and hypoxia, which can lead to the abnormal accumulation of misfolded and unfolded proteins in the ER lumen, a condition referred to as ER stress.[2] The ER stress can trigger the unfolded protein response, which may further cause autophagy or apoptosis.[3] Irrespective of the consequences, current evidence has suggested that reactive oxygen species (ROS), including •OH, $O^{\bullet 2-}$, $ONOO^-$, $H_2O_2$, and $ClO^-$, may be directly or indirectly involved in the ER stress.[4] Unfortunately, the specific role of each kind of ROS in ER homeostasis has not been sufficiently investigated yet. In essence, the lipid nature makes ER to be the main place where lipid peroxidation happens, which is closely related with •OH.[5] However, due to the lack of reliable techniques, the precise association between •OH and ER has not been revealed. Therefore, it is of great importance to develop novel tools to monitor •OH variation in ER.

Nowadays, fluorescent probes have become a powerful tool for detecting ROS in living cells and tissues due to their non-invasiveness, high sensitivity, extraordinary temporal and spatial resolution.[6] Several fluorescent probes have been proposed to study the biological molecular events of •OH in living cells, zebrafish and mice.[7] However, the probe to specifically image •OH in the ER has not been reported yet. The possible reason may be that the targeting strategy for ER is not as clear as that for mitochondria and lysosomes, and the dense lipid microenvironment in ER hinders the capture of •OH by a probe. Hence, developing an endoplasmic reticulum-targeting •OH fluorescent probe is of great value to promote the better understanding of the biological role of •OH in ER stress.

To target ER, two groups including methyl sulphonamide[8] and Pennsylvania Green (PG)[6a,9] are often used due to their appropriate lipophilicity. In this study, we chose PG as the targeting moiety of the probe since PG itself has fluorescence and can indicate the distribution of the probe during the reaction with •OH. Moreover, in our previous study we have developed certain fluorescent probes for monitoring •OH through its hydroxylation of aromatic rings with high selectivity.[10] In the present study, as depicted in Scheme 1, we combined coumarin-3-carboxylic acid (3-CCA), a classical •OH capturing moiety, with PG to construct an ER-targeting •OH probe (EROH). The probe was supposed to react with •OH to yield fluorescent 7-hydroxylcoumarin.[11] With this probe, we have successfully imaged the generation of •OH (through the coumarin channel) in the ER under the inflammation-induced ER stress.

The probe was synthesized in a straightforward manner through two main steps: (1) hexanediamine as a linker was introduced to 3-CCA; (2) the coumarin derivative was coupled to

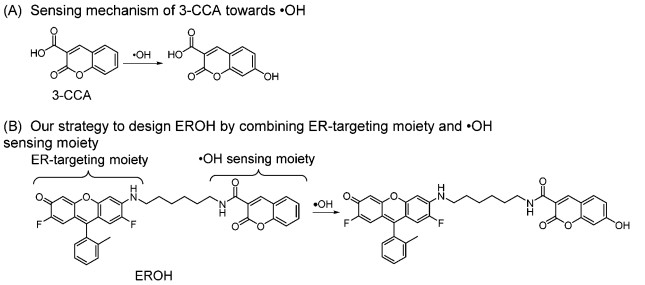


Scheme 1 (A) The sensing mechanism of 3-CCA towards •OH. (B) The design strategy of probe EROH.

[a] *Beijing National Laboratory for Molecular Sciences, Key Laboratory of Analytical Chemistry for Living Biosystems, Institute of Chemistry, Chinese Academy of Sciences, Beijing 100190, China. E-mail: shiwen@iccas.ac.cn, mahm@iccas.ac.cn*
[b] *University of Chinese Academy of Sciences, Beijing 100049, China*

† Electronic supplementary information (ESI) available. See DOI: 10.1039/d0cc00233j

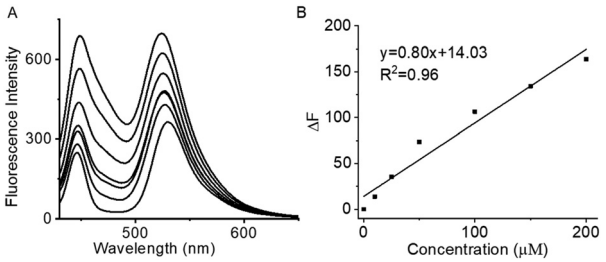


Fig. 1 (A) Fluorescence spectra of EROH (1 μM) with the addition of $H_2O_2$ (curves from bottom to top: 0–600 μM) in the presence of 500 μM $Fe^{2+}$–EDTA. (B) Plot of fluorescence change (Δ*F*) at 446 nm toward the Fenton reagent concentration from 0–200 μM. $\lambda_{ex}$ = 385 nm.

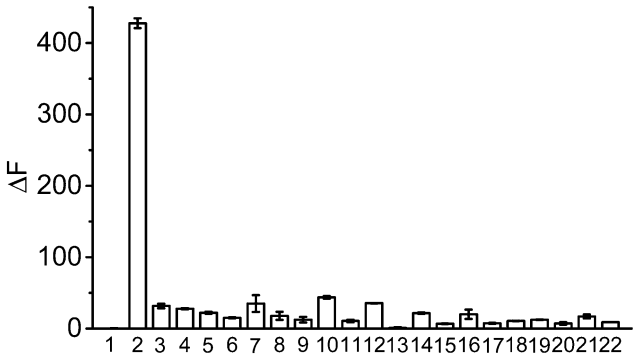


Fig. 2 The fluorescence change of 1 μM EROH at 446 nm toward various species in a pH 7.4 phosphate buffer. (1) Control; (2) 500 μM •OH (500 μM $H_2O_2$ + 500 μM $Fe^{2+}$–EDTA); (3) 150 mM $K^+$; (4) 2 mM $Mg^{2+}$; (5) 500 μM $Fe^{2+}$; (6) 100 μM $Ca^{2+}$; (7) 100 μM $Fe^{3+}$; (8) 100 μM $Cu^{2+}$; (9) 100 μM $Zn^{2+}$; (10) 500 μM $H_2O_2$; (11) 500 μM $^1O_2$ (500 μM $H_2O_2$ + 500 μM $OCl^-$); (12) 500 μM $OCl^-$; (13) 500 μM $ONOO^-$; (14) 500 μM TBHP; (15) 500 μM TBO• (500 μM TBHP + 500 μM $Fe^{2+}$–EDTA); (16) 100 μM $O_2^{\bullet-}$; (17) 5 mM glutathione; (18) 1 mM cysteine; (19) 1 mM glutamic acid; (20) 1 mM alanine; (21) 10 mM glucose; (22) 10 mg $L^{-1}$ bovine serum albumin. $\lambda_{ex/em}$ = 385/446 nm.

PG to obtain the probe EROH. The characterization, including NMR, MS and HPLC, of the probe is described in the ESI† (Fig. S1–S6). Due to the relatively low water solubility, EROH at proper and low concentrations (*e.g.*, 1 μM) was used to study the spectral properties throughout. The fluorescence spectra of EROH before and after the reaction with Fenton's reagent (the most common method to generate •OH in a solution) are shown in Fig. 1A. As is seen, when the amount of •OH increases, the fluorescence at 446 nm increases dependently, which is in accordance with the hydroxylation of the coumarin unit to generate the fluorescent 7-hydroxylcoumarin moiety. The hydroxylation of the probe was also been verified *via* MS analysis ($m/z$ = 625.35 $[M]^+$; Fig. S7, ESI†). In addition, the fluorescence of the PG moiety at 525 nm increases to some extent, which might be ascribed to the concomitant and partial energy transfer from the 7-hydroxylcoumarin to PG moieties. However, the Δ*F* value (the fluorescence difference after and before the reaction of the probe with •OH) at 446 nm is larger than that at 525 nm, suggesting a more sensitive response. Thus, we studied the relationship of fluorescence increase at 446 nm against the varied concentration of •OH that was generated *via* the Fenton reaction ($Fe^{2+}$–EDTA + $H_2O_2$), where the $Fe^{2+}$–EDTA chelate was used to avoid the possible precipitation of $Fe^{2+}$ in a pH 7.4 medium. As shown in Fig. 1B, a good linearity from 10 μM to 200 μM $H_2O_2$ under the constant ferrous concentration is observed with a detection limit (S/N = 3) of 7 μM Fenton's reagent.[10]

Further, the time-course of the fluorescence change of EROH in the absence and presence of •OH was explored. Without •OH, the probe itself displayed a stable fluorescence at 446 nm; when •OH was added, the emission at 446 nm increased immediately and continued rising gradually till 90 min (Fig. S8, ESI†). Subsequently, the fluorescence response of EROH to •OH under different pH values was investigated (Fig. S9, ESI†). In the pH range of 6–10, the probe in the absence of •OH itself exhibited stable fluorescence at 446 nm; in the presence of •OH, large fluorescence enhancement was observed when the media became more alkaline, which can be explained by the fact that the p$K_a$ of 7-hydroxycoumarin is about 7.5.[12] In the nearly neutral environment of ER, EROH may produce relatively strong fluorescence. In addition, since the polarity of ER may be different from that of the aqueous media, we investigated the fluorescence of the probe in various organic solvents with different polarities [including PBS (dielectric constant $\varepsilon$ = 80.1), methanol ($\varepsilon$ = 32.7), ethanol ($\varepsilon$ = 24.6), dichloromethane ($\varepsilon$ = 8.93) and dioxane ($\varepsilon$ = 2.21)], which covered the most biological polarity range.[13] As is seen from Fig. S10 (ESI†), the fluorescence of the probe varies from moderate to acceptable manner.

The selectivity of the probe towards •OH was examined in parallel by testing the potential interfering species in biological system, including metal ions ($K^+$, $Mg^{2+}$, $Fe^{2+}$, $Ca^{2+}$, $Fe^{3+}$, $Cu^{2+}$, and $Zn^{2+}$), other ROS ($H_2O_2$, $^1O_2$, $OCl^-$, $ONOO^-$, TBHP, TBO•, and $O_2^{\bullet-}$), and biological molecules (glutathione, cysteine, glutamic acid, alanine, glucose, and bovine serum albumin). As shown in Fig. 2, the probe EROH exhibits excellent selectivity for •OH over the other species.

The eligible fluorescence property of the probe encourages us to exploit its application to •OH imaging in the cells. The cytotoxicity of the probe EROH was evaluated first *via* The MTT assay (Fig. S11, ESI†). The result showed that the cell viability was not significantly affected upon treatment with the probe EROH up to 5 μM at 37 °C for 24 h, suggesting its low cytotoxicity and good biocompatibility.

Next, the ER-targeting ability of the probe was evaluated by co-staining with commercial dyes. The concentration of 1 μM of EROH was used as well throughout the cell experiment. HeLa cells were co-stained with EROH and ER Tracker Red (ER-Red, a commercial ER-targeting dye). As depicted in Fig. 3, the fluorescence images show that the fluorescence from the green channel (Fig. 3a) overlaps well with that from the red channel (Fig. 3b). A high Pearson's coefficient of 0.99 was observed according to the intensity correlation plot (Fig. 3e). Moreover, the intensity profiles along the cross line in the two channels vary synchronously (Fig. 3f). In contrast, the negative control experiment performed by co-staining the HeLa cells with Mito Tracker Red (Mito-Red, a commercial mitochondrion-targeting dye) or Lyso Tracker Red (Lyso-Red, a commercial lysosome-targeting dye)

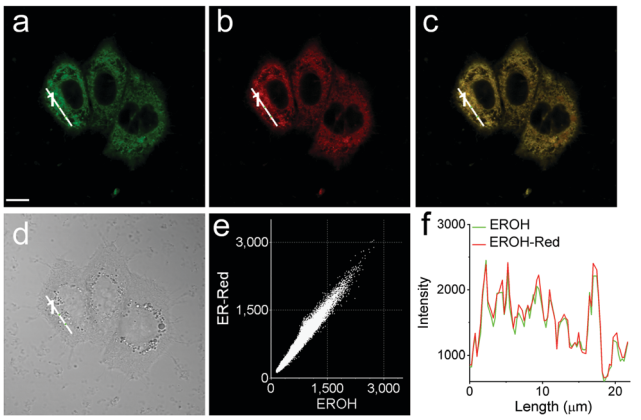


Fig. 3 Co-localization experiments of HeLa cells co-stained with ER-Red (500 nM) and EROH (1 μM). (a) EROH channel (green, $\lambda_{ex}$ = 488 nm, $\lambda_{em}$ = 505–545 nm). (b) ER-Red channel (red, $\lambda_{ex}$ = 559 nm, $\lambda_{em}$ = 580–680 nm). (c) Merged image of (a) and (b). (d) Corresponding differential interference contrast (DIC) image. Scale bar: 10 μm. (e) Intensity correlation plot of ER-Red and EROH. (f) Intensity profiles of the white crossline in the EROH and ER-Red channels.

and EROH gave a poor overlap in the two fluorescence channels with the Pearson's coefficients of 0.65 and 0.36, respectively, as well as an irrelevant change in the intensity profiles of the crosslines (Fig. S12 and S13, ESI†). The above results demonstrate a good endoplasmic reticulum-targeting ability of the EROH in living cells.

Thereafter, EROH was used to image the exogenous •OH in the living cells. In this experiment, the HeLa cells were loaded with EROH first and then treated with various concentrations of the Fenton reagent. As can be seen in Fig. S14 (ESI†), there is little fluorescence in the blue channel in the EROH-loaded HeLa cells before the addition of exogenous •OH. Upon the addition of the Fenton reagent, the fluorescence increases significantly and gradually with increase in the Fenton reagent. To confirm that the fluorescence enhancement resulted from •OH, the specific •OH scavenger, namely 4-hydroxy-2,2,6,6-tetramethylpiperidin-1-oxyl (TEMPOL), was used to pre-treat the EROH-loaded cells before the addition of the Fenton reagent. Such a treatment remarkably inhibited the fluorescence increase (Fig. S14e, ESI†), indicating that fluorescence in the blue channel was indeed due to the •OH reaction.

It has been known that inflammation-induced ROS play an important role in regulating the ER stress.[4b,14] However, the endogenous •OH during this process has not been imaged *in situ*. Thus, we explored the application of EROH for imaging the •OH in ER. Phorbol 12-myristate 13-acetate (PMA) is an effective activator of inflammation for cells and can trigger ER stress as well.[15] As shown in Fig. 4A, after treating the HeLa cells with PMA for 1 h, the cells present significant fluorescence and the fluorescence can be suppressed by TEMPOL, implying the generation of •OH in the ER. In the enlarged images (Fig. 4C), it is seen that the PMA-stimulated cells generate certain discrete spots (image a) in the blue channel; the ER localization image (image b) suggests that these spots are within ER. In principle, abnormal lipid peroxidation caused

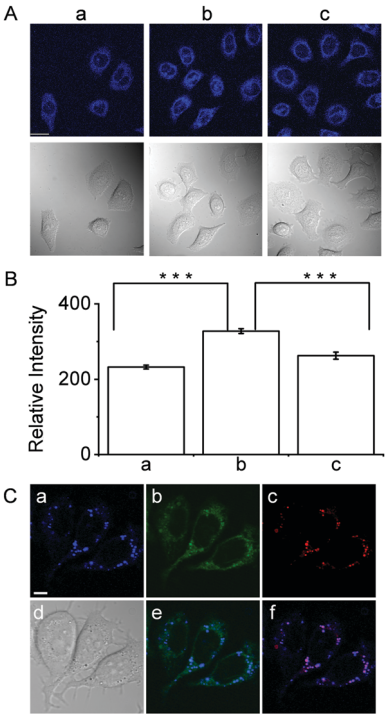


Fig. 4 (A) Confocal fluorescence images of HeLa cells. (a) Cells incubated with EROH (1 μM) for 0.5 h; (b) cells pre-treated with 5 μg mL$^{-1}$ PMA for 1 h, followed by incubation with EROH (1 μM) for 0.5 h; (c) cells pretreated with 5 μg mL$^{-1}$ PMA for 1 h, then incubated with TEMPOL (1 mM) for 0.5 h, and finally incubated with EROH (1 μM) for 0.5 h. The first row is the blue channel of EROH, and the second row is the corresponding DIC images. Scale bar: 20 μm. (B) Relative fluorescence intensity of cells in panel (A). ***$p < 0.001$, **$p < 0.01$, two-side Student's $t$-test. (C) Co-localization experiments of the PMA-treated HeLa cells. Cells were co-stained with EROH (1 μM) and nile red (500 nM). (a) Blue channel for •OH sensing with EROH ($\lambda_{ex}$ = 405 nm, $\lambda_{em}$ = 425–475 nm); (b) green channel for ER targeting with EROH ($\lambda_{ex}$ = 405 nm, $\lambda_{em}$ = 505–545 nm); (c) red channel for nile red ($\lambda_{ex}$ = 559 nm, $\lambda_{em}$ = 580–680 nm); (d) corresponding DIC image; (e) merged image of images (a and b); (f) merged image of images (a and c). Scale bar: 5 μm.

by •OH might lead to the impairment and fracture of ER. The lipid fragment would regroup to form lipid droplets, which would finally be engulfed and degraded in lysosomes, namely ER-phagy.[16] Therefore, we studied the co-localization of the blue spots with lipid droplets (nile red; Fig. 4C) and lysosome (Lyso-Red; Fig. S15, ESI†) dyes. A relatively good fluorescence overlapping (Pearson's coefficient of 0.76) can be detected between the lipid droplets and blue spots, indicating that the blue spots actually present the lipid droplets. For co-localization with Lyso-Red, most spots were isolated in different channels (Fig. S15, ESI†); accordingly, a much lower Pearson's coefficient of 0.40 was obtained. However, we can still find some spots overlapping in both the channels, presumably being the generation of phagosomes. Taken together, the probe EROH may be used to image the function of •OH in the PMA-induced ER stress, revealing that the •OH generation is closely concerned with the lipid droplets formation.

In summary, we have developed EROH as a new ER-targeting fluorescent probe to detect •OH by incorporating coumarin

 

(•OH sensing moiety) with PG (ER-targeting moiety). EROH exhibits a desirable ER-targeting property and •OH sensing ability in cells. The probe has been successfully utilized to image the endogenous •OH and the lipid droplets formation in the ER stress. The analytical performance of EROH may enable it to be used to detect •OH in the endoplasmic reticulum in the •OH-associated diseases.

We thank the financial support from the NSF of China (21922412, 21675159, 21820102007, and 21775152) and Youth Innovation Promotion Association of CAS (2016027).

## Conflicts of interest

There are no conflicts to declare.

## Notes and references

1 (*a*) L. Ellgaard and A. Helenius, *Nat. Rev. Mol. Cell Biol.*, 2003, **4**, 181–191; (*b*) D. Ron and P. Walter, *Nat. Rev. Mol. Cell Biol.*, 2007, **8**, 519–529.
2 (*a*) G. Boden, X. B. Duan, C. Homko, E. J. Molina, W. W. Song, O. Perez, P. Cheung and S. Merali, *Diabetes*, 2008, **57**, 2438–2444; (*b*) Y. M. Zhong, J. M. Li, Y. M. Chen, J. J. Wang, R. Ratan and S. X. Zhang, *Diabetes*, 2012, **61**, 492–504.
3 (*a*) M. Hoyer-Hansen and M. Jaattela, *Cell Death Differ.*, 2007, **14**, 1576–1582; (*b*) I. Tabas and D. Ron, *Nat. Cell Biol.*, 2011, **13**, 184–190.
4 (*a*) J. D. Malhotra and R. J. Kaufman, *Antioxid. Redox Signaling*, 2007, **9**, 2277–2293; (*b*) R. Ozgur, B. Uzilday, Y. Iwata, N. Koizumi and I. Turkan, *J. Exp. Bot.*, 2018, **69**, 3333–3345; (*c*) Z. W. Quan, J. Gu, P. Dong, J. H. Lu, X. S. Wu, W. G. Wu, X. Z. Fei, S. G. Li, Y. Wang, J. W. Wang and Y. B. Liu, *Cancer Lett.*, 2010, **295**, 252–259.
5 (*a*) T. Hallinan, J. Gor, C. A. Rice-Evans, R. Stanley, R. O'reilly and D. Brown, *Biochem. J.*, 1991, **277**, 767–771; (*b*) S. Srivastava and C. Chan, *Free Radical Res.*, 2007, **41**, 38–49.
6 (*a*) K. E. Knewtson, D. Rane and B. R. Peterson, *ACS Chem. Biol.*, 2018, **13**, 2595–2602; (*b*) H. B. Xiao, X. Liu, C. C. Wu, Y. H. Wu, P. Li, X. M. Guo and B. Tang, *Biosens. Bioelectron.*, 2017, **91**, 449–455; (*c*) H. Y. Li, X. H. Li, X. F. Wu, W. Shi and H. M. Ma, *Anal. Chem.*, 2017, **89**, 5519–5525.
7 (*a*) M. J. Kim, S. K. Ko, H. Kim, I. Shin and J. Tae, *Chem. Commun.*, 2013, **49**, 7959–7961; (*b*) L. Y. Zeng, T. Xia, W. Hu, S. Y. Chen, S. Y. Chi, Y. D. Lei and Z. H. Liu, *Anal. Chem.*, 2018, **90**, 1317–1324; (*c*) X. Wang, P. Li, Q. Ding, C. C. Wu, W. Zhang and B. Tang, *Angew. Chem., Int. Ed.*, 2019, **58**, 4674–4678; (*d*) R. L. Zhang, J. Zhao, G. G. Han, Z. G. Liu, C. Liu, C. Zhang, B. H. Liu, C. L. Jiang, R. Y. Liu, T. T. Zhao, M. Y. Han and Z. P. Zhang, *J. Am. Chem. Soc.*, 2016, **138**, 3769–3778; (*e*) W. Q. Feng, Y. Y. Zhang, Z. Li, S. Y. Zhai, W. J. Lv and Z. H. Liu, *Anal. Chem.*, 2019, **91**, 15757–15762; (*f*) Z. Li, T. Liang, S. W. Lv, Q. G. Zhuang and Z. H. Liu, *J. Am. Chem. Soc.*, 2015, **137**, 11179–11185; (*g*) L. X. Li, A. W. Zhu and Y. Tian, *Chem. Commun.*, 2013, **49**, 1279–1281; (*h*) X. Y. Bai, Y. Y. Huang, M. Y. Lu and D. Yang, *Angew. Chem., Int. Ed.*, 2017, **56**, 12873–12877.
8 (*a*) H. B. Xiao, C. C. Wu, P. Li and B. Tang, *Anal. Chem.*, 2018, **90**, 6081–6088; (*b*) H. B. Xiao, P. Li, X. F. Hu, X. H. Shi, W. Zhang and B. Tang, *Chem. Sci.*, 2016, **7**, 6153–6159; (*c*) J. T. Hou, H. S. Kim, C. Duan, M. S. Ji, S. Wang, L. Zeng, W. X. Ren and J. S. Kim, *Chem. Commun.*, 2019, **55**, 2533–2536; (*d*) H. B. Xiao, C. C. Wu, P. Li, W. Gao, W. Zhang, W. Zhang, L. L. Tong and B. Tang, *Chem. Sci.*, 2017, **8**, 7025–7030.
9 (*a*) A. Fujisawa, T. Tamura, Y. Yasueda, K. Kuwata and I. Hamachi, *J. Am. Chem. Soc.*, 2018, **140**, 17060–17070; (*b*) J. M. Meinig, L. Q. Fu and B. R. Peterson, *Angew. Chem., Int. Ed.*, 2015, **54**, 9696–9699.
10 (*a*) H. Y. Li, X. H. Li, W. Shi, Y. H. Xu and H. M. Ma, *Angew. Chem., Int. Ed.*, 2018, **57**, 12830–12834; (*b*) H. Y. Li, W. Shi, X. H. Li, Y. M. Hu, Y. Fang and H. M. Ma, *J. Am. Chem. Soc.*, 2019, **141**, 18301–18307.
11 (*a*) A. Gomes, E. Fernandes and J. L. Lima, *J. Biochem. Biophys. Methods*, 2005, **65**, 45–80; (*b*) S. S. Liu, J. Zhao, K. Zhang, L. Yang, M. T. Sun, H. Yu, Y. H. Yan, Y. J. Zhang, L. J. Wu and S. H. Wang, *Analyst*, 2016, **141**, 2296–2302.
12 P. M. Nowak, F. Sagan and M. P. Mitoraj, *J. Phys. Chem. B*, 2017, **121**, 4554–4561.
13 X. Y. Li, X. H. Li and H. M. Ma, *Chem. Sci.*, 2020, **11**, 1617–1622.
14 K. Z. Zhang and R. J. Kaufman, *Nature*, 2008, **454**, 455–462.
15 M. G. Song, I. G. Ryoo, H. Y. Choi, B. H. Choi, S. T. Kim, T. H. Heo, J. Y. Lee, P. H. Park and M. K. Kwak, *PLoS One*, 2015, **10**, e0134235.
16 S. L. Song, J. Tan, Y. Y. Miao and Q. Zhang, *J. Cell. Physiol.*, 2018, **233**, 3867–3874.